River Flow 2010 - Dittrich, Koll, Aberle & Geisenhainer (eds) - © 2010 Bundesanstalt für Wasserbau ISBN 978-3-939230-00-7

Measuring streambed morphology using range imaging

M. Nitsche, J. M. Turowski, A. Badoux, M. Pauli, J. Schneider, D. Rickenmann
Mountain Hydrology and Torrents Unit, Swiss Federal Research Institute WSL, Birmensdorf, Switzerland

T. K. Kohoutek
Institute of Geodesy and Photogrammetry, Swiss Federal Institute of Technology ETH, Zurich, Switzerland

ABSTRACT: Characterizing streambed morphology is crucial to better understand fluvial systems, since the streambed is an important control on stream dynamics, particle motion and bed stability. There is a lack of data characterizing bed roughness, especially for steep mountain streams. Measurement apparatus like terrestrial laser scanners or airborne Lidar systems are difficult to successfully apply in such environments, because they need free sight, elevated positions and good aerial or road access, which is generally not the case in mountain streams. Moreover, such streams are typically complex in shape and have a wide grain size distribution which complicates measuring with a single method. We present recently available Range Imaging cameras as a novel tool to obtain three-dimensional coordinates of rough surfaces. Mounted on a lightweight crane above the streambed, the cameras generate distance images without significant shadowing effects of large boulders. This experimental study evaluates the precision and the range of applicability of this method. We carried out laboratory and field measurements to get 3D data of artificial and natural surfaces. In the field we realized mean spatial resolution of ~1 cm with distance standard deviations of 7 mm (1σ). Measurement precision degrades with low reflective surfaces or strong illumination contrast at direct sunlight exposure. However, Range Imaging has the potential to generate high resolution data of streambed topography, which is suitable for developing roughness measures.

Keywords: Bed roughness, Streambed morphology, Range Imaging, 3D measurements, Mountain streams

1 INTRODUCTION

Streambed morphology is an important control on stream hydraulics, particle motion and bed stability. Streambeds are rough surfaces that disturb the free flow and offer resistance to it. The characterization of bed roughness is therefore a key to understand fluvial processes. Traditionally total roughness is divided into grain roughness and form roughness. Each distinguishes different scales of roughness, where grain roughness is due to resistance of sand and gravel grains, and form roughness is due to large boulders and bedforms (e.g. Chanson 2004). It is common to describe the grain roughness of the streambed by a single characteristic grain size (Ackers and White 1973, Clifford *et al.* 1992, Gomez 1993, Whiting and Dietrich 1990). Meaningful physical measures to analyze total streambed roughness, such as the standard deviation of surface elevation, have been explored in several studies (Aberle and Smart 2003, Bathurst 1985, Hodge *et al.* 2009a, Nikora *et al.* 1998, Smart *et al.* 2004).

In steep streams, however, the hydraulic roughness of the streambed cannot be sufficiently described by a single grain size (Aberle and Smart 2003). The reason for this is the irregular nature of steep mountain streams, i.e. large and varying bedforms, steep slopes and wide grain size distributions, which result in a significant contribution of form roughness to total roughness (Canovaro *et al.* 2007, Pagliara and Chiavaccini 2006, Rickenmann *et al.* 2006, Yager *et al.* 2007). Difficulties of measuring such complex morphologies have hindered advances in predicting mountain stream hydraulics and sediment transport. Particularly in torrential streams measurements are complicated by vegetation cover, uneven and steep terrain, and difficult access. Characterizing the streambed morphology in the field therefore remains challenging.

Despite these problems, various techniques have been used to characterize fluvial structures.

These include for example physical profilers (e.g. De Jong 1995, Smart *et al.* 2004), photogrammetry (Butler *et al.* 1998, Giménez *et al.* 2009) as well as terrestrial and airborne laser scanning (Cavalli *et al.* 2008, Heritage and Milan 2009, Hodge *et al.* 2009b, Lamarre and Roy 2008, Smart *et al.* 2004). Terrestrial laser scanning (TLS) has proved to be a rapid and precise survey technique feasible to characterize open gravel surfaces (Heritage and Milan 2009, Hodge *et al.* 2009a). However, TLS and other techniques come to their limits if applied in rough terrain. Large boulders in steep mountain streams may obscure a significant portion of streambed surface, even when scanning from different vantage points. Such shadowing effects are smaller when scanning from a bird's eye perspective, which requires lightweight and mobile equipment.

The aim of this study is to develop a mobile, versatile and – compared to TLS – inexpensive survey methodology of total roughness in steep fluvial environments. For this purpose we evaluate the feasibility of recently available Range Imaging (RIM) cameras, which were designed to acquire distance images of close range objects and scenes. We quantify measurement errors under controlled conditions in the field and laboratory. Furthermore, we provide an overview of operating the RIM camera in the field to generate detailed morphological data of a streambed surface.

2 RANGE IMAGING (RIM)

Common methods to measure 3D objects include stereo triangulation, sheet of light triangulation, structured light projection and interferometry. Recently, RIM cameras that capture high resolution distance images at video rate, have been developed. Such cameras measure the distance to an object for each pixel independently, based upon the time-of-flight principle. Time-of-flight can be measured by detecting the time of arrival of a short light pulse which is reflected from an object and received by a sensor, or by measuring the phase shift between the light emitted from a light source and the light received at a sensor.

In this study we used the camera models SR4000 by Mesa Imaging, Switzerland and CamCube by PMDTech, Germany (Table 1), both of which utilize the latter principle.

The RIM cameras use infrared light to illuminate the scene and measure the reflections with a sensor using Complementary Metal Oxide Semiconductor technology (CMOS/CCD) (Lange and Seitz 2001). The emitted light is pulsed at the modulation frequency f_{mod}. The sensor samples the reflected light regularly and calculates the phase shift φ of the modulation with an autocorrelation function (Möller *et al.* 2005).

Since φ is proportional to the target range, it is possible to calculate an absolute target distance by

$$D = \frac{c\varphi}{4\pi f_{mod}}, \quad (1)$$

where c is the speed of light.

In addition to the signal phase shift, the amplitude and the offset can be measured. Here the amplitude indicates the strength of the modulated signal, which is an indication for the measurement accuracy. While the offset represents the local brightness of the scene, i.e. a gray scale value similar to gray scale images.

The maximal non-ambiguity distance range D_{max} is limited to the half of the modulation wavelength λ_{mod}. At a modulation frequency of 20 MHz for the CamCube camera, the modulated wavelength is 15 m. Thus D_{max} is 7.5 m (5.0 m for the SR4000). Distances larger than D_{max} are folded back to the non-ambiguity range. Camera specifications for both devices are listed in Table 1.

Table 1: RIM camera specifications

Model	SR4000	CamCube
Modulation frequency (MHz)	29-31	18-21
Measurement range (m)	0.8-5	0.3-7.5
Sensor pixels	176x148	204x204
Field of view (degree)	43.6x34.6	40x40
Mean resolution at 3 meter (mm)	13.6	10.7
Footprint area at 3 meter (m^2)	4.48	4.77
Camera weight (g)	470	1370
Camera dimensions (mm)	65x65x68	180x194x180
Frame rate ($f\ s^{-1}$)	54	25
Illumination wavelength (nm)	850	870
Price (€)	~5500	~7500

3 EXPERIMENTS TO ESTIMATE ERRORS IN THE DISTANCE DATA

3.1 *Error sources*

So far, there is little experience using RIM to measure complex surfaces in the field. Errors occurring in outdoor use in particular have not been quantified systematically. In this chapter the general constraints of the RIM method and the main sources of errors are investigated to evaluate its scope of application. As with other surveying techniques, random and systematic errors and those originating from maloperation can occur. The error estimation in this section generally refers to raw data, i.e. data have not been processed to enhance quality of the images. The effect of averaging repeated measurements on the data quality is demonstrated below. However, a full treatment

of image processing is not within the scope of this study.

Camera design: Cameras based on phase shift measurements are susceptible to several parameters which produce systematic errors. Some of these parameters are intrinsic to the optical system and to the semiconductor technology. The distance measurement system is affected by the angle of incidence of light, the internal temperature due to self-induced heating, the external temperature, the intensity of reflected beam and the time integration of the light signal (Kahlmann and Ingensand 2005, Kahlmann *et al.* 2006).

Reflectivity, sunlight and water: Since RIM cameras are active optical systems, the accuracy of a distance measurement is directly influenced by the amount of active light which reaches the sensor. Hence, the amplitude of the reflected signal gives a good measure of the accuracy of a distance measurement. Dark and wet surfaces typically have low reflectivity and thus yield poor results. In outdoor application sunlight is much brighter than the active illumination of the camera. This may lead to sensor saturation and increased noise in the distance images and finally to false distance values. Measuring on or through water may be a source for a range of additional errors. The lower velocity of light in water results in an overestimation of distances. Turbulent water may grossly distort the distance image, due to its rapidly changing reflectivity, reflection angle and a possible superposition of solid and fluid surface reflections.

Integration time of the camera: The amount of light that reaches the camera sensor is critical for good data quality. Signal strength depends on the integration time setting of the camera, the reflectivity of the observed object, the strength of the camera's light sources and the amount of background light. Practically, the signal-to-noise-ratio can only be enhanced by adjusting the integration time. If the integration time is too short, the amplitudes, i.e. the signal strength, may be low and the distance values will be noisy. Too long integration times lead to saturation of the sensor and thus to false values.

Pixel footprint: The footprint of each pixel and therefore the image resolution is defined by the distance from the camera to the surface. The side length of each RIM pixel footprint can vary between 4 and 26 mm for the CamCube camera at 1 and 7.5 m distance (divergence angle: 0.1°). For comparison, the beam diameter of typical medium range laser scanners grows little with distance, e.g. from 3 mm at 1 m to 3.3 mm at 7.5 m (divergence angle: 0.013°) for the "Imager 5006i" by Zoller + Fröhlich). This implies that in a single distance image each pixel may represent a different footprint area.

Kahlmann and Ingensand (2005) and Kahlmann *et al.* (2006) give further insights to specific errors of a RIM camera. The authors specify the overall accuracy of distance measurements to be in the range of 1 cm for good conditions, i.e. high target reflectivity and little external light.

3.2 *Laboratory Experiments*

In the experiments described below major types of measurement errors and their magnitudes were investigated under controlled conditions. Tests were conducted in the geodetic calibration laboratory of ETH Zurich with the camera CamCube (Table 1). The camera was fixed facing an even wooden board, which could be moved on a rail to adjust the measuring distance. An interferometer verified the adjusted distance. The board's surface was painted either black or white to achieve two very different levels of reflectivity. External light was reduced to a minimum.

Distance precision at one point of an image: We investigated the precision of distance measurements at the central point of the image for ranges from 1 to 7 meters on both the white and the black board. For each setting the measurement was repeated 250 times. The median of these measurements has shown to equate the independently adjusted camera-target distance and was used as the reference distance. Generally, the variability of measured distances increased with the distance between object and camera. While 90 % of the measurements on the white board deviated less than 0.6 % from the median distance, the measurements on the black board deviated up to 6 % from the median (Fig. 1). For the white board this gives a mean deviation of 3 ± 2 mm (variability gives one standard deviation σ) at 1 m range and 32 ± 25 mm for the 7 m range. Errors for the black board range from 11 ± 8 mm for the 1 m range to 167 ± 124 mm at 5 m.

Variability of distance precision within an image: In another experiment we set up a white and a black board, respectively, at 1 meter range to the camera. Comparing 250 single measurements, the standard deviation of the distance measurements improved towards the center of the image (Fig. 2). For the black board, standard deviation varies from 4 mm at the image center to 142 mm at the outermost edge pixels (image mean 27 mm). Whereas the values for the white board range from 2 to 8 mm (4 mm). These effects can be explained with light scattering within the lens and on the target; this scattering increases with the angle of incidence (Kahlmann and Ingensand 2005). By turning a target in defined angles, a

similar effect has been demonstrated by Kahlmann *et al.* (2006), who showed that the measured distance precision decreases with an increasing angle of incidence.

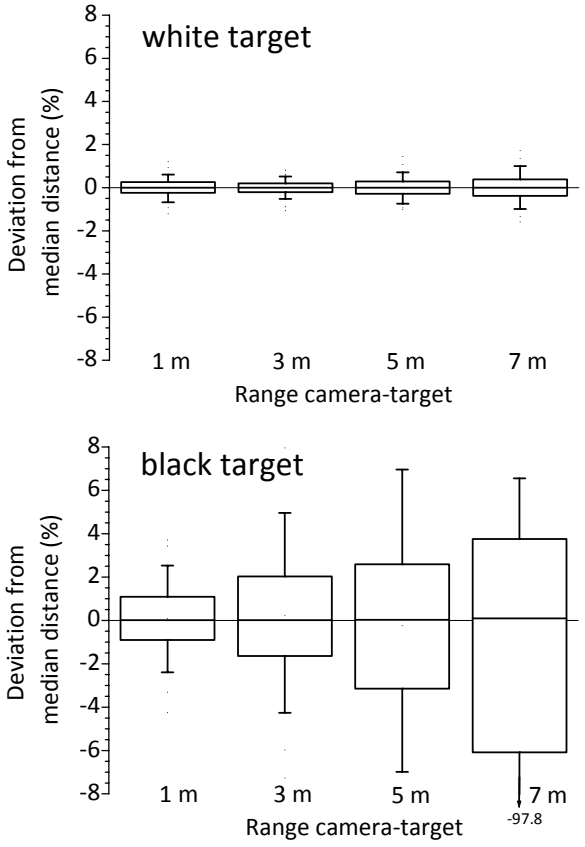

Fig. 1: Measurement precision as a function of distance. Deviation of 250 single measurements from median measured distance per range is shown. The median equates the independently adjusted camera-target distance. Top: High reflectivity target (white board). Bottom: Low reflectivity target (black board). Box defines 25- and 75-percentile and median. Whiskers are 5- and 95-percentile of the data. Measurements were carried out with the camera model CamCube at an integration time of 2500 µs.

Geometric representation of a plane: To investigate the representation of an even plane by the distance images, the white board was set up at 3 m distance from the camera. For a single unprocessed distance image, the standard deviation of the distance data is 14 mm (Fig. 3, dashed lines and grey points). A plane was fitted to the measured points using the least-squares method, giving an absolute mean distance deviation from the plane of 11 ± 9 mm (variability gives one standard deviation σ). By taking the median of 250 repeated measurements for each pixel, the standard deviation of the distance data can be reduced to 7 mm (Fig. 3, straight lines and dark points), leading to a mean distance deviation from the plane of 5 ± 4 mm. Data towards the edges of the image scattered more and appeared to be further away from the camera. Reasons for this overestimation of distances at the edges might be: (i) vignetting,

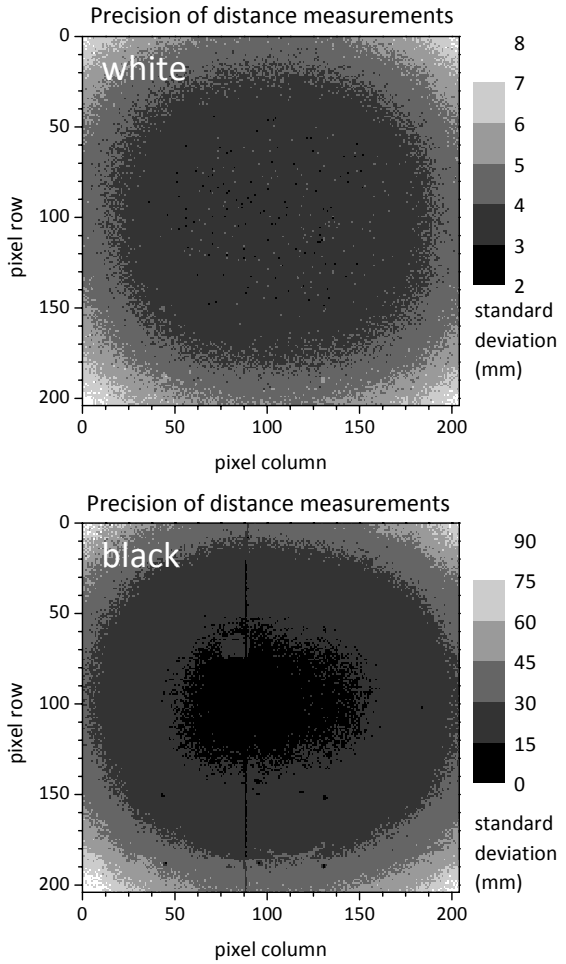

Fig. 2: Distribution of measurement precision across the camera sensor. Shown are standard deviations of 250 repeated distance measurements against a plane board, positioned normal to the camera at 1 m range. Columns and rows represent values for each pixel of the camera sensor. Captured area is ~0.7 m x 0.7 m. Top: High reflectivity target (white board). Bottom: low reflectivity target (black board). Note the difference in scale in top and bottom of the figure. Measurements were carried out with the CamCube camera using an integration time of 2500 µs.

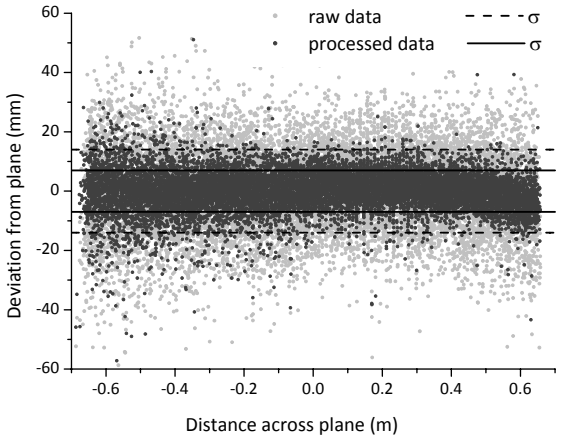

Fig. 3: Distance measurements of a planar surface. The measured plane was an even white board, positioned normal to the camera at 3 m range. A measurement of perfect accuracy would give a value of zero for all points. Grey points show the vertical distance of the measured point from the plane. Black points show the median vertical distance of 250 repeated measurements. Lines give variability as one standard deviation σ. Measurements were carried out with the CamCube camera using an integration time of 2500 µs.

which is the reduction of the image's brightness or saturation at the periphery compared to the image center, and (ii) spherical aberration, which is the increased refraction of light near the lens edge.

3.3 *Field experiments with varying light conditions*

We also tested RIM cameras under natural conditions outdoors in a mountain river streambed. The aim was to qualitatively evaluate the camera performance under different natural lighting conditions and to investigate the effects of water and wet rock surfaces on the measurements. The camera was mounted on a crane looking vertically down to the ground (Fig. 4). The same footprint area was repeatedly measured, with light conditions ranging from direct sunlight exposure at mid day to almost no natural light at night.

The quality of single distance measurements clearly varied with lighting conditions. Measurements at night revealed the greatest details of the surface, whereas the image became obscured by noise under direct sunlight exposure (Fig. 5). The increase in noise with increased light exposure can be illustrated by comparing the standard deviations of measured distances from the mean surface height. While the standard deviation evaluates to 36.63 cm for direct sunlight conditions (Fig. 5, d), it reduces to 17.13 cm for shady conditions and to 10.7 cm at night (Fig. 5, c, b). The noise within a single measurement under direct sunlight is thus of a similar magnitude as the total surface relief (92 cm), precluding the distinction of single cobbles or rocks.

On one hand, turbulent water scattered the light, which led to large variations in the distance image (Fig. 5, a-d, left part, respectively.). Flat water surfaces on the other hand allowed the modulated light to penetrate and measure approximately the sub water surface of the riverbed (Fig. 5, a-d, mid bottom). However, the influence of water on image quality cannot currently be quantified. Water surfaces should thus be omitted from further surface analysis.

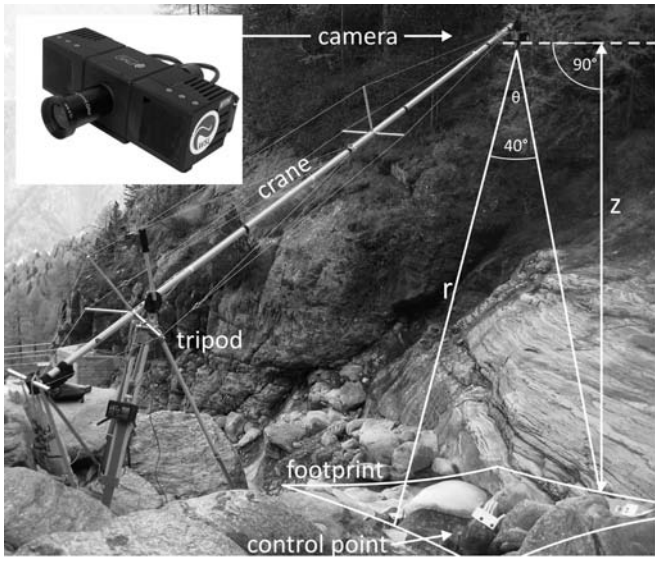

Fig. 4: Crane with mounted camera over streambed. The footprint is the area in the cameras field of view; r is the measured spherical distance of one pixel of the camera sensor; z is the calculated orthogonal distance to the camera; θ is the aperture angle of the camera, which is 40° for the shown camera. Crane arm length is 5.2 m. Coordinates of the control points (steel targets) are measured with a total station, enabling a camera data transformation to the global coordinate system. Inset: CamCube camera (Table 1).

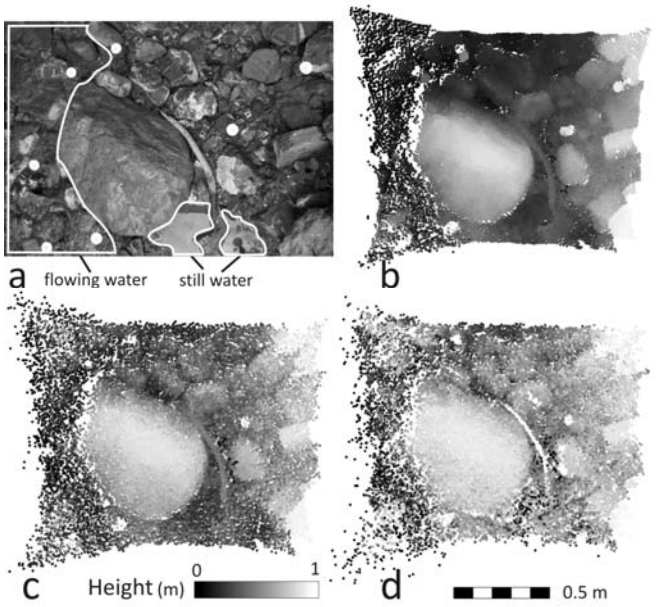

Fig. 5: Top view image and point clouds of a gravel bed surface. The mapped area is ~1.6 m x 1.2 m with a point density of 1 point cm^{-2} near the image center. a) Image showing one large boulder sitting on gravel and rocks. White polygons display water surfaces. b-d) point clouds measured at different light conditions: b) no light at night, c) shaded daylight, d) direct sunlight. The designated heights refer to a local reference (the minimum local height of b). Measurements were carried out with the SR4000 camera using an integration time of 2000 µs.

To identify errors under natural lighting, we repeated the measurement of an even plane in the outdoors. Instead of a white board, as used to generate the data shown in Fig. 3, a cardboard box was used. Since the geometry was known independently, spatial variations of measurement precision could be calculated. Here we present the

distance data of one planar side of the cardboard box (Fig. 6).

For a single unprocessed distance image, the standard deviation of the distances equals 20 mm (Fig. 6, dashed lines, grey points). A plane was fitted to the measured points using the least-squares method. The absolute mean distance deviation from this plane is 16 ± 12 mm (variability gives one standard deviation σ). As shown in Fig. 3, the data precision can be considerably improved by taking the median of a number of repeated measurements pixel by pixel. In this example, 134 replicate measurements resulted in a reduced standard deviation of 7 mm (Fig. 6, straight lines, black points). The processed distances have then a mean deviation from the plane of 5 ± 5 mm. The precision of the processed data is hence in the same range as results from a similar experiment in the laboratory (Fig. 3).

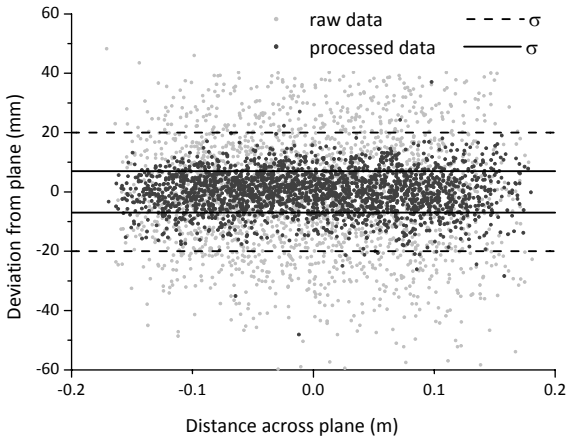

Fig. 6: Distance measurements of a planar surface in daylight conditions. The measured plane was one side of a grey cardboard box facing the camera at 2 m distance with an angle of 40°. Sunlight was bright but the scene was shaded. A measurement of perfect accuracy would give the result "0" for all points. Grey points show the vertical distance of the measured point from the plane. Black points show the median vertical distance of 134 repeated measurements. Lines give variability as one standard deviation σ. Measurements were carried out with the CamCube camera using an integration time of 2500 µs.

4 OUTLOOK TO FIELD APPLICATION

In this section an example is given of how to apply RIM in the field to generate a high resolution Digital Terrain Model (DTM) of a small streambed section, which in future can be developed and applied to an entire stream reach.

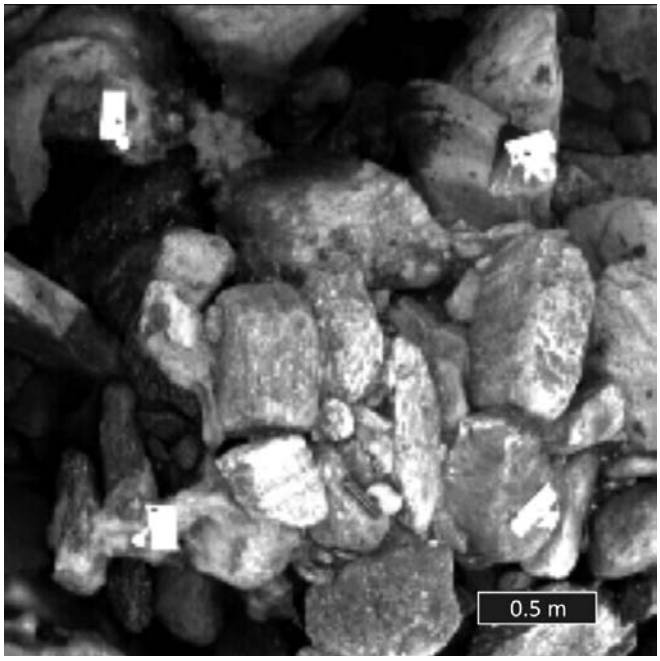

Fig. 7: Greyscale image of the CamCube camera footprint, simultaneously taken with the distance image. Displayed are boulders, flowing water (dark shading), and control points with labels (white rectangles). The captured area is 2.7 m x 2.7 m. Largest boulders are 50 cm in diameter (b-axis). See also Fig. 8.

To realize a top view of the surface, the camera was mounted on a commercial lightweight camera crane (Fig. 4). Turning and moving the crane allowed capturing larger areas, such as a streambed reach of interest. In this case, overlapping the camera footprints by 30-50 % simplified data assembly during post-processing.

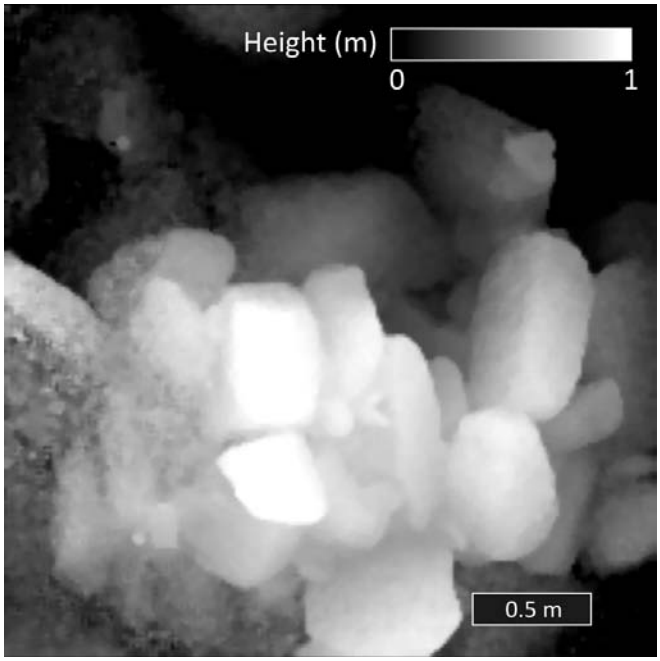

Fig. 8: DTM derived from CamCube camera footprint. The area is same as shown in Fig. 7. Height is relative to the lowest point of the footprint. The point density near the center of the image is 0.6 point cm^{-2}. The integration time of the CamCube camera was 2500 µs.

Fig. 7 and Fig. 8 show an example greyscale image and the calculated DTM of a footprint. The quality of the distance data was enhanced by averaging 30 repeated distance measurements and filtering the resulting distance image with a 3x3 matrix median filter to remove outliers and implausible values.

To merge multiple footprints to a single point cloud of the scanned section, four control points were placed in each footprint and their global coordinates were measured with a total station. This allowed the transformation of the local camera coordinates to global coordinates. Instead of using control points, it is also possible to merge the footprints via a best fit iterative closest point algorithm (e.g. Besl and McKay 1992). The merged point cloud can then be used to derive a DTM with standard interpolation techniques.

5 DISCUSSION

The experiments carried out in the laboratory and in the field aimed to investigate the potential of RIM to acquire surface data of steep riverbeds and to quantify the main measurement errors. The dominant error sources appear to be random errors due to the sensitivity of the camera to early and multiple reflections of the emitted light. This leads to a large variability in repeated distance measurements. The reflectivity of the surveyed surface also has an impact on data precision. The latter problem can be mitigated by adjusting the integration time of the sensor, which also allows to get a strong signal from dark low reflective surfaces.

Errors can generally be reduced by an order of magnitude by measuring the same scene repeatedly and averaging the distance data (cf. sections 3.2, 3.3; Fig. 3; Fig. 6). The median of repeated distance measurements has shown to be closest to the actual independently measured distance. This enables the use of the median for final coordinate calculation.

Compared to ~2 mm distance precision observed for TLS (Hodge *et al.* 2009b) and 2-10 mm for photogrammetry methods (Butler *et al.* 1998, Carbonneau *et al.* 2003, Chandler *et al.* 2001), the distance data of the tested RIM cameras gave a precision of 7 mm for averaged data generated in the laboratory, with mean absolute distance deviations of 5 ± 4 mm. The precision of the tested RIM cameras has thus shown to be similar to other instruments for high resolution surface measurements.

RIM measurements showed generally larger variability in the field (20 mm) than in the laboratory (7 mm). However, the standard deviation could also be reduced to 7 mm by taking the median values of multiple images (here we used 134 images). The mean absolute distance deviation from the reference object was 5 ± 5 mm. Since RIM cameras can operate in a video mode at 25 frames per second, a large number of images can be obtained easily and quickly. It took a mere 5 s to capture the data used for averaging in this study, and a larger number of pictures would lead to further improved precision. In addition, data quality might be further optimized by more sophisticated data processing algorithms. This potential has to be evaluated in further studies.

The spatial resolution of RIM distance data depends solely on the camera-to-target distance. In our examples of field measurements (sections 3.3 and 4) point densities of 1 point cm^{-2} and 0.6 point cm^{-2} could be realized. At this resolution, grains with sizes larger than 5 cm can be clearly and unambiguously identified. At smaller grain sizes the signal-to-noise ratio is too small to reliably differentiate structures. This limit, however, appears to be appropriate for developing roughness measures in steep streams, which are dominated by gravel, large boulders, and bedforms.

To avoid shadowing effects of large grains, which may hide portions of the streambed, a vertical view of the streambed is highly desirable. Due to the small size and weight of RIM cameras it is easy to mount the camera on a crane or an overhead gantry system (Fig. 4). This is a major advantage compared to TLS. Moreover, the weight and dimension of the camera also allows to measure in remote and steep terrain without road access.

For some applications it might be interesting to repeat capturing a scene to assess detailed surface changes or to study measurement accuracy. While with TLS repeated measurements never hit the same point, fixed RIM cameras always produce distance data for exactly the same footprint, because ray angles do not change due to a static optical lens.

In addition, the video mode of RIM cameras allows the measurement of rapidly moving surfaces, a task TLS cannot currently achieve.

6 CONCLUSION

In this study a new method to acquire 3D coordinates of rough streambed surfaces is presented. While for plane gravel surfaces (and referred grain roughness) TLS appears to be a feasible technique (Heritage and Milan 2009, Hodge *et al.* 2009a, Hodge *et al.* 2009b), RIM provides an alternative method that can be applied also on

rough, bouldery surfaces. RIM cameras are lightweight, relatively inexpensive and can produce high resolution distance and greyscale images. It is important to post-process the distance data to reduce a variety of measurement errors. Finally, DTMs of stationary and moving surfaces can be derived from the RIM data, which are useful to investigate streambed roughness in steep mountain channels.

ACKNOWLEDGEMENTS

This study was supported by the Swiss Federal Office for the Environment. We thank A. Volkwein for his C++ programming support, and P. Thee, B. Fritschi, H. Hastedt, and R. Hegglin for technical and field assistance.

REFERENCES

Aberle, J. and Smart, G.M., 2003. The influence of roughness structure on flow resistance on steep slopes. Journal of Hydraulic Research, 41(3): 259-269.

Ackers, P. and White, W.R., 1973. Sediment transport: new approach and analysis. Journal of the Hydraulics Division, Proceedings of ASCE, 99(HY11): 2041-2060.

Bathurst, J.C., 1985. Flow resistance estimation in mountain rivers. Journal of Hydraulic Engineering, 111(4).

Besl, P.J. and McKay, N.D., 1992. A method for registration of 3-d shapes. IEEE Trans. Pat. Anal. and Mach. Intel., 14(2): 239-256.

Butler, J.B., Lane, S.N. and Chandler, J.H., 1998. Assessment of DEM quality for characterizing surface roughness using close range digital photogrammetry. Photogrammetric Record, 16(92): 271-291.

Canovaro, F., Paris, E. and Solari, L., 2007. Effects of macro-scale bed roughness geometry on flow resistance. Water Resources Research, 43(W10414).

Carbonneau, P., Lane, S. and Bergeron, N., 2003. Cost-effective nonmetric close-range digital photogrammetry and its application to a study of coarse gravel river beds. International Journal of Remote Sensing, 24(14): 2837-2854.

Cavalli, M., Tarolli, P., Marchi, L. and Dalla Fontana, G., 2008. The effectiveness of airborne LiDAR data in the recognition of channel-bed morphology. Catena, 73(3): 249-260.

Chandler, J., Shiono, K., Rameshwaren, P. and Lane, S., 2001. Measuring flume surfaces for hydraulics research using a Kodak DCS460. Photogrammetric Record, 17(97): 39-61.

Chanson, H., 2004. The Hydraulics of Open Channel Flow. Butterworth-Heinemann, Oxford, 630 pp.

Clifford, N.J., Robert, A. and Richards, K.S., 1992. Estimation of flow resistance in gravel-bedded rivers: a physical explanation of the multiplier of roughness length. Earth Surface Processes and Landforms, 17: 111-126.

De Jong, C., 1995. Temporal and spatial interactions between river bed roughness, geometry, bed load transport and flow hydraulics in mountain streams - Examples from Squaw Creek (Montana, USA) and Lainbach/Schmiedlaine (Upper Bavaria, Germany). Geographische Abhandlungen, 59: 1-229.

Giménez, R. *et al.*, 2009. Accuracy of high-resolution photogrammetric measurements of gullies with contrasting morphology. Earth Surface Processes and Landforms, 34(14): 1915-1926.

Gomez, B., 1993. Roughness of stable, armored gravel beds. Water Resources Research, 29(11): 3631-3642.

Heritage, G.L. and Milan, D.J., 2009. Terrestrial Laser Scanning of grain roughness in a gravel-bed river. Geomorphology, 113: 4-11.

Hodge, R., Brasington, J. and Richards, K., 2009a. Analysing laser-scanned digital terrain models of gravel bed surfaces: linking morphology to sediment transport processes and hydraulics. Sedimentology, 2009(56): 2024–2043.

Hodge, R., Brasington, J. and Richards, K., 2009b. In situ characterization of grain-scale fluvial morphology using Terrestrial Laser Scanning. Earth Surface Processes and Landforms, 34(2009): 954-968.

Kahlmann, T. and Ingensand, H., 2005. Range Imaging Sensor Properties and Calibration. Proceedings of the 1st Range Imaging Research Day at ETH Zurich, Switzerland.

Kahlmann, T., Remendino, F. and Ingensand, H., 2006. Calibration for Increased Accuracy of the Range Imaging Camera SwissRanger. , TM Proceedings of the ISPRS Com. V Symposium, Dresden, Germany.

Lamarre, H. and Roy, A.G., 2008. A field experiment on the development of sedimentary structures in a gravel-bed river. Earth Surface Processes and Landforms, 33: 1064-1081.

Lange, R. and Seitz, P., 2001. Solid-State, Time-of-Flight Range Camera. IEEE Journal of Quantum Electronics.

Möller, T., Kraft, H., Frey, J., Albrecht, M. and Lange, R., 2005. Robust 3D measurements with PMD sensors, Proceedings of the 1st Range Imaging Research Day at ETH Zurich, Zurich, Switzerland.

Nikora, V.I., Goring, D.G. and Biggs, B.J.F., 1998. On gravel-bed roughness characterization. Water Resources and Research, 34(3): 517-527.

Pagliara, S. and Chiavaccini, P., 2006. Flow Resistance of Rock Chutes with Protruding Boulders. Journal of Hydraulic Engineering, 132(6).

Rickenmann, D., Chiari, M. and Friedl, K., 2006. SETRAC – A sediment routing model for steep torrent channels. In: R. Ferreira, E. Alves, J. Leal and A. Cardoso (Editors), River Flow 2006. Taylor & Francis Group, London.

Smart, G., Aberle, J., Duncan, M. and Walsh, J., 2004. Measurement and analysis of alluvial bed roughness. Journal of Hydraulic Research, 42(3): 227-237.

Whiting, P.J. and Dietrich, W.E., 1990. Boundary shear stress and roughness over mobile alluvial beds. Journal of Hydraulic Research, 116: 1495-1511.

Yager, E.M., Kirchner, J.W. and Dietrich, W.E., 2007. Calculating bed load transport in steep boulder bed channels. Water Resources Research, 43(W07418).